Contrib Mineral Petrol (2009) 158:113–130
DOI 10.1007/s00410-008-0373-2

ORIGINAL PAPER

Origin of a Mesozoic granite with A-type characteristics from the North China craton: highly fractionated from I-type magmas?

Neng Jiang · Shuangquan Zhang · Wenge Zhou · Yongsheng Liu

Received: 20 August 2008 / Accepted: 29 December 2008 / Published online: 21 January 2009

Abstract We report geochronological, geochemical and isotopic data for the Mesozoic Shangshuiquan granite from the northern margin of the North China craton. The granite is highly fractionated, with $SiO_2 > 74\%$. Occurrence of annitic biotite, high contents of alkalis ($K_2O + Na_2O$), Rb, Y, Nb and heavy rare earth elements, high FeO_t/MgO, low contents of CaO, Al_2O_3, Ba, and Sr, and large negative Eu anomalies, makes it indistinguishable from typical A-type granites. A mantle-derived origin for the rocks of the granite is not favored because their high initial $^{87}Sr/^{86}Sr$ (≥ 0.706) and low ε_{Nd} (t) (< -15) are completely different from either those of the lithospheric or asthenospheric mantle. In fact, their Sr–Nd isotopes fall within the range of Sr–Nd isotopic compositions of the Archean granulite terrains and are comparable to those of Mesozoic crustal-derived I-type granitoids in the region. Therefore, the Shangshuiquan granite is considered to be dominantly derived from partial melting of the ancient lower crust. Its parental magmas prove to be similar to I-type magmas and to have undergone extensive fractionation during its ascent. This is supported by the fact that some of the nearby Hannuoba feldspar-rich granulite xenoliths can be indeed regarded as the early cumulates in terms of their mineralogy, chemistry, Sr–Nd isotopes and zircon U–Pb ages and Hf isotopes. It is furthermore argued that some of highly fractionated granites worldwide, especially those with A-type characteristics and lacking close relationship with unfractionated rocks, may in fact be fractionated I-type granites. This suggestion can explain their close temporal and spatial associations as well as similar Sr–Nd isotopes with I-type granites. Our study also sheds new light on the petrogenesis of deep crustal xenoliths.

Keywords Fractionation · I-type granite · A-type granite · North China craton · Lower crustal xenoliths

Communicated by T.L. Grove.

N. Jiang (✉)
Key Laboratory of Mineral Resources, Institute of Geology and Geophysics, Chinese Academy of Sciences, Beijing, China
e-mail: jiangneng@mail.iggcas.ac.cn

S. Zhang
Department of Chemistry and Biochemistry, University of Windsor, Windsor, ON, Canada

W. Zhou
Institute of Geochemistry, Chinese Academy of Sciences, Guiyang, China

Y. Liu
State Key Laboratory of Geological Processes and Mineral Resources, China University of Geosciences, Wuhan, China

Introduction

Granitic rocks and their volcanic equivalents are the most abundant constituents of the upper crust. Approximately 20 different schemes have been proposed to classify granites over the past several decades (e.g., Chappell and White 1974; Barbarin 1999; Frost et al. 2001). Among these, a widely used classification scheme is that of Chappell and White (1974), which subdivides granites into I-type and S-type. There are also volumetrically minor "A"-(alkaline, anhydrous, and anorogenic) and "M" (mantle-like)-type granites, which are essentially subcategories of the I-types. Since A-type granites are considered to be emplaced in intraplate or anorogenic setting (Loiselle and Wones 1979) and have distinctive geochemical characteristics, i.e., high contents of alkalis ($Na_2O + K_2O$), Zr, Nb, Ga, Y, and REE

(except Eu), and low contents of Al_2O_3, CaO, Ba, Sr, and Eu and therefore high elemental ratios, such as Ga/Al and FeO_{total}/MgO (Collins et al. 1982; Whalen et al. 1987; Eby 1990; Creaser et al. 1991), a number of chemical discrimination diagrams have been put forward to distinguish A-type from other types of granites (Whalen et al. 1987; Eby 1990; Frost et al. 2001). However, in felsic granites ($SiO_2 > 74\%$), the chemical and mineralogical composition of different granite types converge and many of the characteristics of A-type granites can also be achieved by extensive fractionation of other types of granites. As a result, for granites with $SiO_2 > 74\%$, it is essentially impossible to classify them using the various chemical discrimination diagrams.

Here we report elemental and isotopic characteristics of a highly fractionated Mesozoic granite with A-type features from the Zhangjiakou region at the northern margin of the North China craton. In the same region, there are three Mesozoic I-type granitoids and they are considered to be derived from the ancient lower crust (Jiang et al. 2007). This provides a good opportunity to evaluate the genetic relationships between the Shangshuiquan granite and these I-type granitoids. In addition, various types of granulite xenoliths entrained in the Hannuoba basalts near the Shangshuiquan granite provide a unique opportunity to examine whether some of them represent early cumulates from the parent magmas of the granite, resulting in the highly fractionated nature of the Shangshuiquan granite.

Geological setting

The North China craton (Fig. 1) preserves crustal remnants as old as 3.8 Ga (Liu et al. 1992). It has been commonly accepted that the sub-continental lithospheric mantle beneath the eastern part of the North China craton has experienced a dramatic change from a Paleozoic cratonic mantle to a Cenozoic "oceanic" lithospheric mantle, accompanied by considerable thinning of the lithosphere during the Phanerozoic (Menzies et al. 1993; Griffin et al. 1998). At the same time, the eastern part of the craton has experienced widespread tectonothermal reactivation, as indicated by emplacement of voluminous granitoids and extensive volcanism.

The Zhangjiakou region is tectonically situated at the northern margin of the intervening Trans-North China orogen which along with the Eastern and Western blocks constitute the North China craton (Fig. 1). The Precambrian basement rocks are widely distributed in the area, which have been considered to represent an exposed lower crust section (Zhai 1996). Phanerozoic magmatic rocks in the region are widespread, consisting of a Devonian Shuiquangou syenitic complex (Miao et al. 2002), the voluminous Mesozoic intrusive and extrusive rocks as well as the Cenozoic Hannuoba basalts which cover an area of about 1,700 km^2. Abundant xenoliths derived from the lower crust and mantle lithosphere have been found in the Hannuoba basalts (Chen et al. 2001). The lower crustal

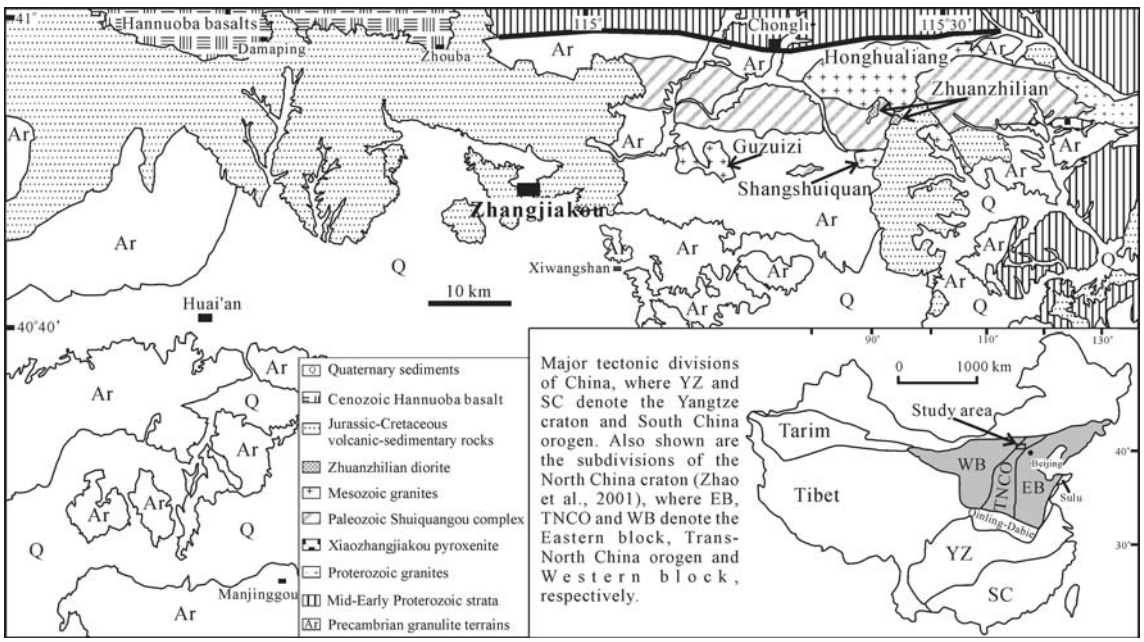

Fig. 1 Simplified geological map of the Zhangjiakou region showing the distribution of the Shangshuiquan A-type granite, the Mesozoic I-type granitoids, the Hannuoba basalts and the Precambrian basement rocks. The Hannuoba feldspar-rich granulite xenoliths are collected from Damaping and Zhouba

xenoliths include felsic, intermediate and mafic granulites, with mafic and intermediate xenoliths greatly outnumbering felsic granulites (Wilde et al. 2003). The intermediate-mafic granulite xenoliths can be broadly classified into two types: feldspar-rich and pyroxene-rich.

Mesozoic intrusive rocks

The Shangshuiquan granite is the main object of this paper. For comparison, three additional Mesozoic plutons are also discussed. They are the Zhuanzhilian diorite, the Honghualiang granite and the Guzuizi granite. Rocks from these three plutons possess adakite-like characteristics (Jiang et al. 2007) and they are collectively referred to as I-type granitoids hereafter.

The Shangshuiquan granite is exposed in an area of about 8 km^2. Rocks of the granite are pink and leucocratic with medium-grained granitic texture. The rocks mainly are composed of quartz, orthoclase, and plagioclase, with minor interstitial biotite. Magnetite, zircon and apatite are accessory.

The Zhuanzhilian diorite is dark gray and has been dated at 139.5 ± 0.9 Ma by SHRIMP U–Pb zircon methods (Jiang et al. 2007). Its distribution area is unclear due to poor exposure. Rocks of the Zhuanzhilian diorite are composed of orthopyroxene, clinopyroxene, biotite, amphibole, plagioclase, and quartz and minor K-feldspar, magnetite and ilmenite, with accessory apatite, zircon and titanite.

The Honghualiang granite is exposed in an area of about 96 km^2. The rocks show an even, medium-grained granitic texture and are composed of quartz, orthoclase, and plagioclase, with minor biotite and accessory magnetite and zircon. The Honghualiang granite has been dated at 235 ± 2 Ma by SHRIMP U–Pb zircon methods (Jiang et al. 2007).

The Guzuizi granite is exposed in an area of about 20 km^2. A salient feature of the granite is that euhedral–subhedral perthite occurs as phenocrysts with size typically >2 cm. The Guzuizi granite has been dated at 236 ± 2 Ma by SHRIMP U–Pb zircon methods (Miao et al. 2002).

Analytic methods

U–Pb dating

Zircons U–Pb analyses were conducted with laser ablation ICP-MS. Cathodoluminescence images were made of the zircons before analyses. The dating was conducted on an Agilent 7500a ICP-MS equipped with a 193 nm laser at the State Key Laboratory of Geological Processes and Mineral Resources, China University of Geosciences, Wuhan. The analytical procedure is described in Yuan et al. (2004). During analysis, the spot diameter was 32 μm. U, Th and Pb concentrations were calibrated by using ^{29}Si as the internal calibrant and NIST 610 as the reference material. The $^{207}Pb/^{206}Pb$ and $^{206}Pb/^{238}U$ ratios were calculated using the GLITTER program, which were then corrected using the zircon 91500 as external calibrant. The age calculations and plotting of concordia diagrams were made using ISOPLOT (ver 3.0) (Ludwig 2003).

Mineral analysis

Major element compositions of minerals were measured on a Cameca SX51 electron microprobe at the Institute of Geology and Geophysics, Chinese Academy of Sciences, using an accelerating voltage of 15 kV, beam current of 20 nA and spot diameter of 5 μm.

Major and trace element analysis of bulk rocks

Major element compositions were measured by X-ray fluorescence (XRF) using fused glass disks at Institute of Geology and Geophysics. Trace element composition was determined by ICP-MS (Finnigan Element) at Institute of Geology and Geophysics and ICP-MS (Agilent7500a) at China University of Geosciences, Wuhan, respectively. Analyses of rock standards indicate precision and accuracy typically are better than 10% for the trace elements.

Sr–Nd isotopes

Samples were digested in Teflon bombs after being spiked with ^{84}Sr, ^{87}Rb, ^{150}Nd and ^{147}Sm tracers before $HF + HNO_3$ dissolution. Rb, Sr, Sm and Nd were separated using conventional ion exchange procedures, and were measured using a Finnigan MAT 262 thermal ionization multi-collector mass spectrometer at the Laboratory for Radiogenic Isotope Geochemistry, the Institute of Geology and Geophysics, Chinese Academy of Sciences, Beijing, China. Procedural blanks were <100 pg for Sm and Nd and <500 pg for Rb and Sr. The measured $^{143}Nd/^{144}Nd$ and $^{87}Sr/^{86}Sr$ ratios were normalized to $^{146}Nd/^{144}Nd = 0.7219$ and $^{86}Sr/^{88}Sr = 0.1194$, respectively.

The BCR-2 standard measured during the course of the analyses gave an average $^{143}Nd/^{144}Nd$ of 0.512613 ± 0.000012 (2σ), $^{147}Sm/^{144}Nd = 0.1380$, Nd = 28.67 ppm Sm = 6.55 ppm, $^{87}Sr/^{86}Sr = 0.7040973 \pm 0.000013$ (2σ), $^{87}Rb/^{86}Sr = 0.3827$, Rb = 44.05 ppm and Sr = 340.5 ppm.

We calculate depleted mantle Sm–Nd model ages (T_{DM}^{Nd}) for the Shangshuiquan granite assuming linear isotopic growth for a depleted mantle reservoir from $\varepsilon_{Nd}(T) = 0$ at 4.55 Ga to $\varepsilon_{Nd}(0) = 10$ ($^{143}Nd/^{144}Nd = 0.51315$) at present, with $^{147}Sm/^{144}Nd = 0.2137$. The equations used are:

$$\varepsilon_{Nd} = \left[\left(^{143}Nd/^{144}Nd\right)_S / \left(^{143}Nd/^{144}Nd\right)_{CHUR} - 1\right] \times 10{,}000$$

$$f_{Sm/Nd} = \left[\left(^{147}Sm/^{144}Nd\right)_S / \left(^{147}Sm/^{144}Nd\right)_{CHUR}\right] - 1$$

$$T_{DM}^{Nd} = 1/\lambda \ln\left\{1 + \left[\left(^{143}Nd/^{144}Nd\right)_S - 0.51315\right] / \left[\left(^{147}Sm/^{144}Nd\right)_S - 0.2137\right]\right\}$$

where s = sample, and $(^{143}Nd/^{144}Nd)_{CHUR} = 0.512638$, $(^{147}Sm/^{144}Nd)_{CHUR} = 0.1967$, and $\lambda_{Sm} = 6.54 \times 10^{-12}$ year^{-1} (Lugmair and Marti 1978; Jacobsen and Wasserburg 1980; Goldstein et al. 1984).

Hf isotopes of zircons

In situ zircon Hf isotopic analyses were conducted using the Neptune MC-ICP-MS, equipped with a 193 nm laser at the Institute of Geology and Geophysics, Chinese Academy of Sciences, Beijing, China. The detailed analytical technique is described in Wu et al. (2006). During analyses, the $^{176}Hf/^{177}Hf$ and $^{176}Lu/^{177}Hf$ ratios of the standard zircon (91500) were 0.282300 ± 0.000018 ($2\sigma_n$, $n = 13$) and 0.000316, similar to the commonly accepted $^{176}Hf/^{177}Hf$ ratio of 0.282284 ± 0.000003 (1σ) measured using the solution method (Woodhead et al. 2004).

We have used a decay constant for $\lambda_{Lu} = 1.867 \times 10^{-11}$ year^{-1} (Soderlund et al. 2004) and the $^{176}Hf/^{177}Hf$ and $^{176}Lu/^{177}Hf$ ratios of average chondrite and estimated depleted mantle at the present day are 0.282772 and 0.0332, and 0.28325 and 0.0384, respectively (Blichert-Toft and Albarede 1997). We use $T_{DM}^{Hf,C}$ model ages to represent the age for the source of the host magma of the zircon, which is derived by projecting the initial $^{176}Hf/^{177}Hf$ of the zircon back to the depleted mantle model growth curve, assuming a mean crustal value for Lu/Hf ($^{176}Lu/^{177}Hf = 0.015$; Griffin et al. 2002).

Results

Geochronology

Zircons from the Shangshuiquan granite sample JN0743 are euhedral and stubby. They are mainly between 120 and 180 μm long and are homogeneous or have oscillatory zones in the CL images (Fig. 2). The LA-ICP-MS analytical results are presented in Table 1 and Fig. 3. Nineteen points form a coherent group with a weighted mean $^{206}Pb/^{238}U$ age of 142.9 ± 0.8 Ma (Fig. 3) which is in good agreement with the previous SHRIMP age of 142.2 ± 1.3 Ma (Miao et al. 2002). This age indicates that the Shangshuiquan granite is marginally older than the nearby Zhuanzhilian diorite which yields a SHRIMP age of 139.5 ± 0.9 Ma (Jiang et al. 2007).

Mineral chemistry

Mineral chemistry of the Shangshuiquan granite is listed in Table 2. For comparison, mineral chemistry of the Hannuoba feldspar-rich and pyroxene-rich granulite xenoliths is also listed in Table 2. Plagioclase from the Shangshuiquan granite is sodic (An numbers are typically of <4), whereas plagioclase from the feldspar-rich granulite xenoliths is andesine. K-feldspar from the Shangshuiquan granite is almost pure orthoclase. Biotite from the Shangshuiquan granite is annitic, with Mg# lower than 5 (Table 2).

Major and trace elements

The rocks from the Shangshuiquan granite are metaluminous to peraluminous, with A/CNK and A/NK ratios ranging from 0.93 to 1.03 and from 1.02 to 1.08, respectively. They show most of the characteristics of the typical

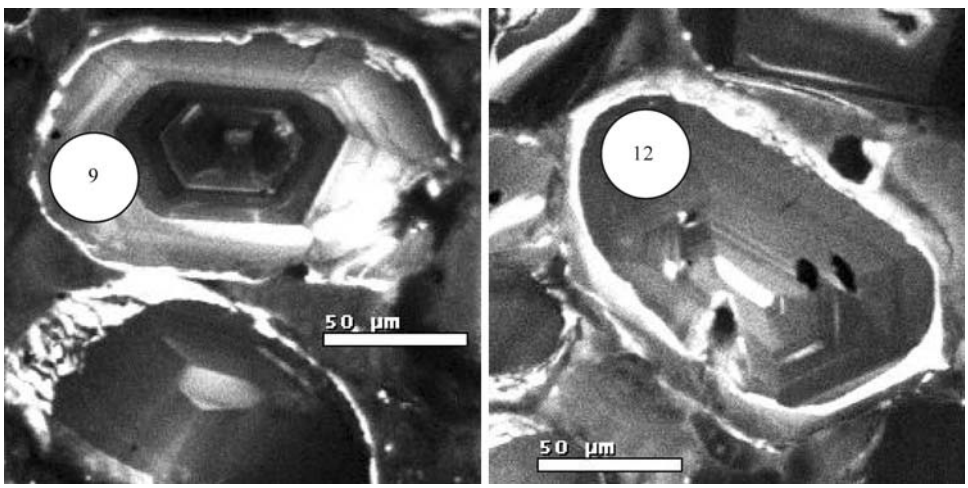

Fig. 2 Cathodoluminescence (CL) images of representative zircons from the Shangshuiquan granite. The *solid circles* indicate the locations of LA-ICP-MS U–Pb analyses and the numbers refer to the analytical spots in Table 1

Table 1 Zircon LA-ICP-MS analyses of the Shangshuiquan granite (JN0743)

	Concentrations (ppm)				Isotopic ratios						Ages (Ma)	
	Pb	U	Th	Th/U	$^{207}Pb/^{206}Pb$	1σ	$^{207}Pb/^{235}U$	1σ	$^{206}Pb/^{238}U$	1σ	$^{206}Pb/^{238}U$	1σ
1	35.4	1,067	800	0.75	0.0496	0.0012	0.1491	0.0033	0.0218	0.0002	139	1
3	144.2	4,231	3,122	0.74	0.0518	0.0010	0.1613	0.0028	0.0226	0.0002	144	1
4	28.1	852	561	0.66	0.0507	0.0012	0.1563	0.0036	0.0224	0.0002	143	1
5	74.2	2,288	1,270	0.55	0.0537	0.0019	0.1625	0.0054	0.0220	0.0002	140	1
6	96.7	2,770	2,481	0.90	0.0489	0.0010	0.1520	0.0029	0.0226	0.0002	144	1
8	63.1	1,875	1,354	0.72	0.0536	0.0013	0.1669	0.0039	0.0226	0.0002	144	1
9	24.4	719	595	0.83	0.0485	0.0013	0.1505	0.0038	0.0225	0.0002	143	1
10	89.5	2,862	1,392	0.49	0.0485	0.0011	0.1500	0.0031	0.0224	0.0002	143	1
11	101.0	2,944	2,527	0.86	0.0509	0.0011	0.1582	0.0032	0.0226	0.0002	144	1
12	98.1	2,822	2,654	0.94	0.0509	0.0011	0.1586	0.0034	0.0226	0.0002	144	1
13	48.1	1,481	1,058	0.71	0.0512	0.0012	0.1564	0.0036	0.0222	0.0002	141	1
15	94.0	2,760	2,354	0.85	0.0515	0.0012	0.1593	0.0036	0.0224	0.0002	143	1
16	132.5	3,995	2,975	0.74	0.0503	0.0012	0.1561	0.0035	0.0225	0.0002	144	1
18	113.8	3,236	3,272	1.01	0.0496	0.0012	0.1536	0.0036	0.0225	0.0002	143	1
19	37.1	1,199	688	0.57	0.0490	0.0014	0.1505	0.0041	0.0223	0.0002	142	1
20	78.4	2,449	1,571	0.64	0.0485	0.0013	0.1516	0.0038	0.0227	0.0002	145	1
21	61.7	1,970	1,141	0.58	0.0530	0.0014	0.1650	0.0043	0.0226	0.0002	144	2
22	49.3	1,570	980	0.62	0.0543	0.0015	0.1677	0.0045	0.0224	0.0002	143	2
23	106.0	3,287	2,387	0.73	0.0516	0.0014	0.1590	0.0041	0.0224	0.0002	143	1

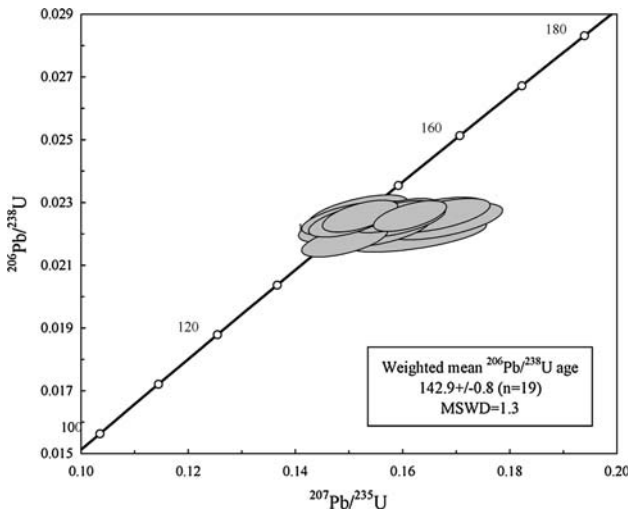

Fig. 3 Zircon LA-ICP-MS U–Pb concordia diagram of the Shangshuiquan granite

A-type granite, such as high contents of alkalines (i.e., high $K_2O + Na_2O$ with $K_2O/Na_2O > 1$), Rb, Y, Nb and heavy rare earth elements (HREE), high Fe* (Fe* = $FeO_t/(FeO_t + MgO)$), low contents of CaO, Al_2O_3, Ba, and Sr (Table 3). The relative enrichment of HREE (La_N/Yb_N = 3.5–5.7, with one exception of 10.8) has produced a relatively flat chondrite-normalized REE pattern with a large negative Eu anomaly (Fig. 4), which is characteristic of A-type granites in New England Fold Belt, Australia (Landenberger and Collins 1996).

Below we examine the geochemical characteristics of rocks of the Shangshuiquan granite in more detail, and compare them to the Hannuoba feldspar-rich granulite xenoliths and rocks of the three Mesozoic I-type granitoids. On the diagram of Fe* versus SiO_2 (Frost et al. 2001), rocks of the Shangshuiquan granite and one feldspar-rich xenolith are iron-enriched, whereas the rest rocks are magnesian (Fig. 5). Three of the xenoliths are particularly magnesium-enriched with Fe* $\leq$ 0.5.

Whole rock Sr–Nd and zircon Hf isotopic data

Measured whole rock Sr and Nd isotopic ratios for the Shangshuiquan granite are given in Table 3. Isotopic ratios have been calculated at 140 Ma. Rocks of the Shangshuiquan granite have high $(^{87}Sr/^{86}Sr)_i$ (0.706–0.709) and low ε_{Nd} (t) (−15.6 to −16.5), essentially similar to those of the feldspar-rich granulite xenoliths and the I-type granitoids (Fig. 6). They all fall within the range of Sr–Nd isotopic compositions of the Precambrian granulite terrains and are completely different from either those of the lithospheric mantle-derived Hannuoba peridotite xenoliths (Rudnick et al. 2004) or those of the asthenospheric mantle-derived Hannuoba basalts (Song et al. 1990).

Table 2 Mineral chemistry of the Shangshuiquan granite and the Hannuoba feldspar-rich and pyroxene-rich granulite xenoliths

	Shangshuiquan granite				Hannuoba feldspar-rich granulite xenoliths										Pyroxene-rich xenoliths		
Sample	JN73				DMP-508			DMP-01				91ZH2[a]			95DA15[a]		
Mineral	Bt $n = 6$	Pl $n = 5$	Ksp $n = 3$	Mt $n = 2$	Cpx $n = 3$	Opx $n = 3$	Pl $n = 3$	Ilm $n = 2$	Cpx $n = 6$	Opx $n = 5$	Pl $n = 2$	K-spar $n = 1$	Mt $n = 1$	Ilm $n = 1$	Cpx $n = 1$	Pl $n = 2$	Cpx	Opx	Pl
SiO_2	34.62	67.78	64.18	–	50.13	50.03	59.02	–	50.44	51.24	60.79	65.55	0.10	–	50.93	61.22	49.74	51.48	53.88
TiO_2	1.26	–	0.03	0.32	0.45	0.12	0.04	46.66	0.55	0.10	0.01	0.05	27.33	52.40	0.29	0.01	0.82	0.18	0
Al_2O_3	17.84	20.25	18.69	0.47	4.58	2.80	25.55	0.35	4.75	2.68	23.32	18.72	2.49	0.14	2.48	23.91	5.98	4.37	28.08
FeO	30.39	0.05	0.29	91.07	12.12	27.37	0.25	47.64	11.89	25.12	0.13	0.09	62.84	42.21	10.06	0.13	6.33	16.68	0.04
MnO	1.39	0.02	–	0.25	0.28	0.60	0.04	0.38	0.28	0.56	0.00	–	0.54	0.54	1.03	0.01	0.11	0.3	0
MgO	0.80	–	0.01	–	11.26	18.71	0.02	4.48	11.39	20.11	0.01	–	3.07	3.87	12.49	–	13.26	25.94	0.03
CaO	0.03	0.40	–	–	19.85	0.55	7.41	0.04	19.36	0.78	5.93	0.68	–	–	20.76	5.62	21.05	0.48	11.1
Na_2O	0.12	11.19	0.56	–	1.07	0.05	6.42	–	1.43	0.06	6.73	4.39	–	–	1.15	7.13	0.92	–	4.95
K_2O	8.99	0.17	16.07	–	–	–	1.26	–	–	0.01	2.33	9.86	–	–	–	1.68	–	–	0.05
Total	95.44	99.86	99.83	92.11	99.76	100.24	100.01	99.55	100.08	100.68	99.25	99.34	96.36	99.17	99.19	99.69	98.21	99.43	98.13
T (°C)					840				848						899				

Temperature (T) is calculated using the 2-pyroxene geothermometer of Wood and Banno (1973)

Bt biotite, *Pl* plagioclase, *Ksp* K-feldspar, *Cpx* clinopyroxene, *Opx* orthopyroxene, *Ilm* ilmenite, *Mt* magnetite

[a] Data from Chen et al. (1998, 2001)

On the diagram of ε_{Nd} (t) and $^{147}Sm/^{144}Nd$, rocks of the Shangshuiquan granite are significantly different from those of the feldspar-rich granulite xenoliths and the I-type granitoids in $^{147}Sm/^{144}Nd$ ratios (Fig. 7). Most samples of the Shangshuiquan granite plot to the right of the linear array defined by the exposed granulites and amphibolites that presumably represent the lower crustal source rocks of the Mesozoic I-type granitoids in the region (Jiang et al. 2007). The rest rocks all plot to the left of the linear array.

Hf isotopic data of zircons for the Shangshuiquan granite and one feldspar-rich granulite xenolith (DMP-06) are listed in Table 4. The Shangshuiquan granite and the xenolith have almost identical ε_{Hf} (t) and $T_{DM}^{Hf, C}$ model ages, which are also similar to those of the I-type granitoids (Jiang et al. 2007) (Fig. 8).

Dignostic signatures of the A-type granites?

A number of chemical discrimination diagrams have been put forward to distinguish A-type from other types of granites (Whalen et al. 1987; Eby 1990; Frost et al. 2001). High Ga/Al ratios and Zr + Nb + Y + Ce values are considered the most diagnostic features for A-type granites (Whalen et al. 1987). However, high Ga/Al ratios can also be achieved in highly fractionated I-type and S-type granites (Whalen et al. 1987). For example, an average of 64 samples of highly fractionated felsic I-type granites from the Lachlan Fold Belt (Chappell and White 1992) falls into the A-type field in the Ga/Al versus $K_2O + Na_2O$, FeO_t/MgO, Zr and Nb diagrams (Fig. 9). This is also true for some of the fractionated I-type granites from northeastern China (Wu et al. 2002). On the other hand, due to extensive fractionation, the felsic end-member of the A-type suite may contain low contents of Zr + Nb + Y + Ce, plotting out of the A-type field (e.g., the leucogranites of the Chaelundi A-type suite, Fig. 10). Moreover, A-type granites are usually considered to have higher FeO_t/MgO than I-type granites. In fact, the difference in FeO_t/MgO between A- and I-type granites is only manifest at $SiO_2 < 70\%$, and when $SiO_2 > 70\%$, the FeO_t/MgO of the two types of granites overlaps significantly (Frost et al. 2001). It is clear that many of the characteristics for A-type granites can also be achieved by extensive fractionation of I-type granites. Therefore, the various chemical discrimination diagrams cannot effectively distinguish strongly fractionated A-type granites from similarly fractionated I-type granites. At present, classification of very felsic rocks can only be made confidently when there is an association with less evolved rocks within the same suite (King et al. 1997).

Below, we examine whether the A-type characteristics of the Shangshuiquan granite are produced by extensive

Table 3 Chemical and Sr–Nd isotopic compositions of the Shangshuiquan granite

	JN72	JN73	JN74	JN75	JN0743	JN0746	JN0747	JN0749
SiO_2	76.95	77.1	76.62	76.84	77.39	76.76	77.28	74.68
TiO_2	0.07	0.06	0.07	0.06	0.07	0.06	0.07	0.13
Al_2O_3	11.86	12.16	12.02	11.98	12.20	12.26	12.23	13.03
Fe_2O_3	1.05	1.00	1.09	0.98	1.24	1.24	1.15	1.47
MnO	0.04	0.04	0.05	0.04	0.03	0.04	0.04	0.03
MgO	0.06	0.07	0.08	0.07	0.07	0.06	0.06	0.17
CaO	0.58	0.42	0.39	0.43	0.27	0.28	0.19	0.41
Na_2O	4.04	4.10	3.88	3.95	4.09	4.13	3.96	4.12
K_2O	4.63	4.39	4.58	4.49	4.34	4.53	4.62	4.92
P_2O_5	0.01	0.01	0.01	0.01	0.01	0.02	0.01	0.03
LOI	0.68	0.92	0.67	0.75	0.26	0.18	0.22	0.32
Total	99.97	100.27	99.46	99.60	99.98	99.56	99.83	99.31
Mg#	10.2	12.2	12.7	12.4	10.1	8.7	9.4	18.6
Tzr (°C)	786	764	797	779	784	757	787	847
T_{Apt} (°C)	776	777	773	775	795	807	794	833
Zn	60.5	102.4	85.7	79.8	33.4	42.3	42.0	17.9
Ga	24.0	22.6	23.1	23.4	22.0	22.7	22.2	21.5
Rb	257.4	233.3	248.3	247.2	236	284	267	253
Sr	12.6	22.5	10.3	18.1	15.8	11.0	15.8	109
Y	54.2	35.3	58.3	45.6	39.4	29.1	13.4	18.9
Zr	172.0	122.6	178.4	146.2	149	112	154	154
Nb	55.4	38.8	57.8	47.2	47.6	40.0	54.6	28.9
Ba	6.2	42.0	14.5	28.6	34.6	36.0	31.9	318
La	25.8	27.5	25.4	26.8	22.2	16.9	15.5	35.8
Ce	65.1	68.2	63.7	67.4	56.5	38.3	40.0	80.7
Pr	7.72	7.88	7.67	7.81	6.88	5.71	4.39	8.35
Nd	28.9	28.0	29.2	28.3	26.4	22.4	15.6	28.9
Sm	7.61	6.44	7.78	6.87	6.82	5.79	3.09	5.27
Eu	0.08	0.09	0.09	0.09	0.098	0.064	0.058	0.34
Gd	7.55	5.66	7.64	5.98	6.01	4.79	2.22	3.96
Tb	1.32	0.93	1.35	1.01	1.20	0.98	0.42	0.67
Dy	7.90	5.34	8.01	5.98	6.82	5.23	2.50	3.57
Ho	1.62	1.06	1.71	1.22	1.36	1.06	0.56	0.73
Er	4.79	3.18	4.86	3.56	3.85	2.84	1.76	2.02
Tm	0.72	0.49	0.78	0.55	0.62	0.46	0.32	0.35
Yb	4.67	3.28	4.81	3.67	4.18	3.23	2.42	2.23
Lu	0.65	0.45	0.7	0.52	0.60	0.45	0.36	0.30
Hf	6.84	5.13	7.43	5.94	6.97	5.61	7.72	5.73
Ta	3.27	2.63	3.51	2.95	2.88	3.07	3.57	2.32
Pb	24.81	18.47	23.8	19.5	30.5	23.2	26.5	31.1
Th	38.6	23.4	35.8	25.4	27.7	21.2	25.0	25.3
U	4.1	3.1	3.8	3.2	3.46	2.90	4.17	3.56
Eu/Eu*	0.03	0.04	0.04	0.04	0.05	0.04	0.07	0.23
$^{87}Rb/^{86}Sr$	56.01	29.06	59.52	40.64	42.10	72.17	48.12	6.76
$^{87}Sr/^{86}Sr$	0.820178	0.763848	0.827419	0.787067	0.791822	0.850018	0.801660	0.721833
2σ	12	7	13	13	14	17	23	14
$(^{87}Sr/^{86}Sr)i$	0.708719	0.706019	0.708976	0.706194	0.708038	0.706400	0.705901	0.708384
$^{147}Sm/^{144}Nd$	0.1581	0.1385	0.1638	0.1542	0.1568	0.1658	0.1252	0.1042

Table 3 continued

	JN72	JN73	JN74	JN75	JN0743	JN0746	JN0747	JN0749
$^{143}Nd/^{144}Nd$	0.51176	0.511748	0.51181	0.511792	0.511769	0.511790	0.511738	0.511751
2σ	11	6	13	10	10	14	11	9
$(^{143}Nd/^{144}Nd)_i$	0.511612	0.511618	0.511660	0.511651	0.511626	0.511638	0.511624	0.511656
$\varepsilon Nd(t)$	−16.5	−16.3	−15.6	−15.8	−16.2	−16.0	−16.3	−15.7
T_{DM}^{Nd} (Ma)	3,777	2,826	4,052	3,451	3,666	4,281	2,420	1,942

The $(^{87}Sr/^{86}Sr)_i$, $(^{143}Nd/^{144}Nd)_i$ and $\varepsilon Nd(t)$ are recalculated at t = 140 Ma. Tzr (°C)-zircon saturation temperature is calculated using the geothermometer of Watson and Harrison (1983); the T_{Apt} (°C)-apatite saturation temperature is calculated using the geothermometer of Harrison and Watson (1984)

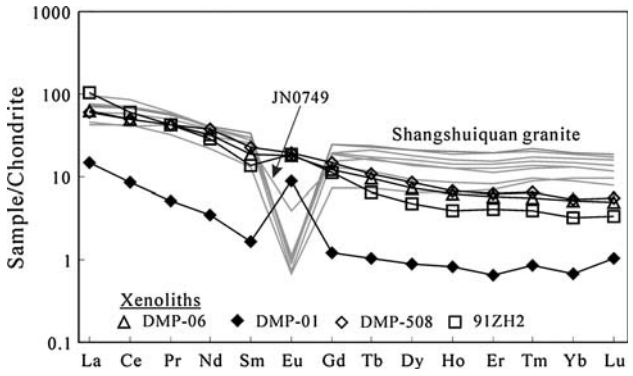

Fig. 4 Chondrite-normalized REE patterns of the Shangshuiquan granite and the Hannuoba feldspar-rich granulite xenoliths. Normalizing values from Sun and McDonough (1989). Data of the Hannuoba feldspar-rich granulite xenoliths are from Zhang (1997) and Liu et al. (2001, 2004, 2005)

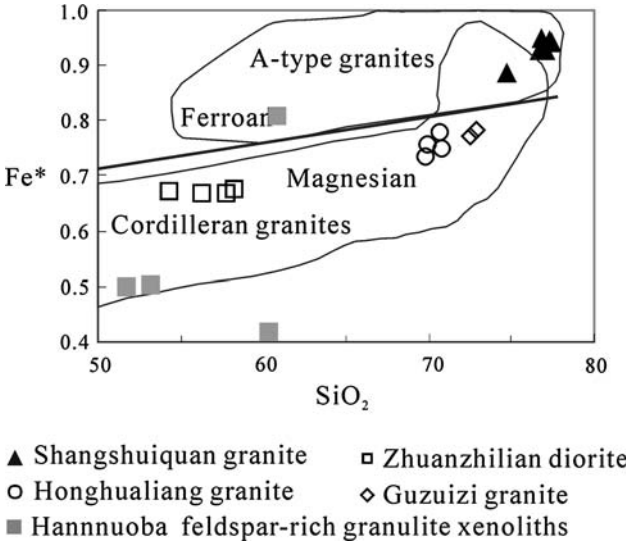

Fig. 5 Whole-rock Fe* ($FeO_t/(FeO_t + MgO)$) versus SiO_2 (wt%) diagram shows composition of the Shangshuiquan granite. Fe* line, magnesian Cordilleran granites and A-type granites fields are from Frost et al. (2001). Data of the Honghualiang granite, the Guzuizi granite and the Zhuanzhilian diorite are from Jiang et al. (2007) and data source of the feldspar-rich granulite xenoliths is the same as in Fig. 4

fractionation of I-type magmas and whether some of the nearby Hannuoba feldspar-rich granulite xenoliths are the early cumulates.

Xenoliths as products of fractional crystallization

Various granulite xenoliths have been found from the Tertiary Hannuoba alkaline basalts near the Shangshuiquan granite. They are diverse in both chemical and isotopic compositions (Liu et al. 2001, 2004, 2005). Detailed examinations of the intermediate-mafic xenoliths reveal that the feldspar-rich granulite xenoliths are mineralogically and chemically different from the pyroxene-rich granulite xenoliths that have been considered to have a restite origin (Jiang et al. 2007). The feldspar-rich xenoliths are dominated by plagioclase and K-feldspar with various abundance of quartz. Orthopyroxene and/or clinopyroxene are minor along with Fe–Ti oxides. Zircon is an accessory phase. The pyroxene-rich granulite xenoliths are dominated by clinopyroxene and orthopyroxene with subordinate plagioclase ± garnet.

Compared to the pyroxene-rich xenoliths, the feldspar-rich xenoliths contain much higher potassium. This is particularly evident in the xenolith 91ZH2 (4.84 wt% K_2O). Since all the Mesozoic granitoids are potassium-rich, the restites should be potassium-poor. It is thus unlikely that the feldspar-rich xenoliths represent restites generated by melting of the source rocks to produce these potassium-rich Mesozoic magmas. On the other hand, since K is highly incompatible during partial melting, it is expected that the refractory residue should be depleted in K. We preclude the feldspar-rich xenoliths as refractory residue. Instead, the enrichment of K in the feldspar-rich xenoliths can result from fractionation of potassium feldspar during magma ascent.

The feldspar-rich granulite xenoliths are significantly different from the pyroxene-rich granulite xenoliths in

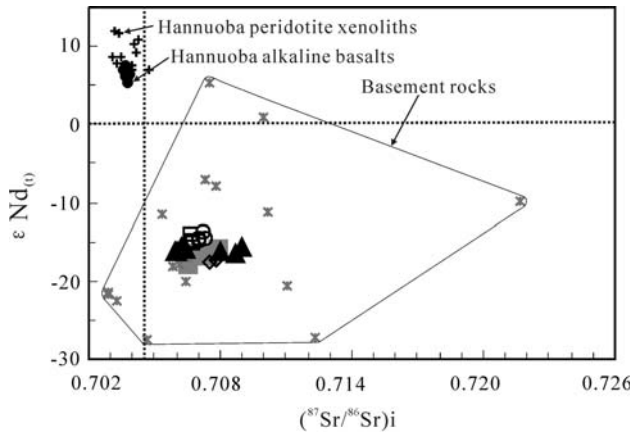

Fig. 6 Initial $^{87}Sr/^{86}Sr$ versus $^{143}Nd/^{144}Nd$ values (calculated at 140 Ma) of the Shangshuiquan granite and Hannuoba feldspar-rich xenoliths. Symbols are the same as in Fig. 5. Data for the Hannuoba peridotite xenoliths from Rudnick et al. (2004), the Hannuoba alkaline basalts from Song et al. (1990) and the rest are the same as in Fig. 5

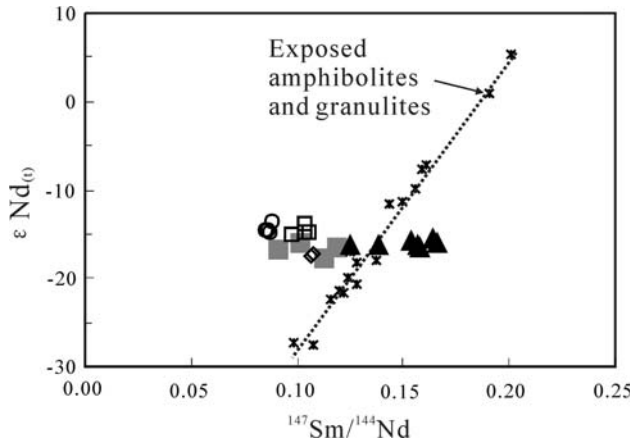

Fig. 7 ε_{Nd} (t) versus $^{147}Sm/^{144}Nd$ for rocks for the Shangshuiquan granite and Hannuoba feldspar-rich xenoliths. ε_{Nd} (t) are recalculated at 140 Ma. Symbols are the same as in Fig. 5. Source of data is the same as in Fig. 5. The *dashed line* is a mathematical regression

mineral chemistry (Table 2). Clinopyroxene, orthopyroxene and plagioclase in the feldspar-rich xenoliths all contain lower Al_2O_3 that their counterparts in the pyroxene-rich xenoliths. In addition, in the feldspar-rich xenoliths, plagioclase has lower *An* numbers and clinopyroxene and orthopyroxene have lower MgO than their counterparts in the pyroxene-rich xenoliths (Table 2). The different mineral chemistry between the two types of xenoliths requires them being treated separately.

A distinguishing feature of the feldspar-rich granulite xenoliths is their extremely low concentrations of Cr and Ni despite of their high Mg# (Liu et al. 2001, 2005). In fact,

Table 4 Zircon Hf isotopes of the Shangshuiquan granite and one feldspar-rich xenolith

	$^{206}Pb^a/^{238}U$ age (Ma)	$^{176}Lu/^{177}Hf$	$^{176}Hf/^{177}Hf$	2σ	$\varepsilon_{Hf}(t)$	$T_{DM}^{Hf,\ C}$ (Ma)
Hannuoba granulite xenolith (DMP-06)[a]						
1	98	0.000197	0.282145	19	−20.0	2,417
2	91	0.000139	0.282175	22	−19.1	2,354
3	102	0.000344	0.282180	22	−18.7	2,338
4	89	0.000412	0.282138	22	−20.5	2,437
5	106	0.000064	0.282141	20	−20.0	2,421
6	111	0.000237	0.282175	20	−18.7	2,344
7	112	0.000404	0.282111	22	−20.9	2,483
8	122	0.000018	0.282168	18	−18.7	2,351
9	122	0.000608	0.282190	18	−18.0	2,306
10	130	0.000635	0.282152	20	−19.1	2,385
11	101	0.000525	0.282150	22	−19.8	2,406
12	100	0.000614	0.282149	17	−19.9	2,407
13	143	0.000144	0.282124	16	−19.8	2,436
14	145	0.000078	0.282166	18	−18.3	2,343
15	81	0.000449	0.282163	19	−19.8	2,386
16	145	0.000530	0.282117	16	−20.0	2,453
17	146	0.000467	0.282138	20	−19.3	2,406
18	146	0.000439	0.282152	19	−18.8	2,375
19	146	0.000617	0.282170	15	−18.2	2,337
20	146	0.000060	0.282156	16	−18.6	2,363
Shangshuiquan granite (JN0743)						
1		0.002501	0.282175	16	−18.3	2,340
4		0.002566	0.282140	14	−19.5	2,417
5		0.003167	0.282200	14	−17.4	2,288
6		0.003179	0.282194	19	−17.7	2,303
8		0.003196	0.282164	15	−18.7	2,369
9		0.001608	0.282176	14	−18.1	2,332
11		0.002984	0.282157	15	−19.0	2,383
12		0.003331	0.282135	13	−19.8	2,433
13		0.003264	0.282210	16	−17.1	2,267
14		0.004253	0.282189	14	−18.0	2,320
15		0.003159	0.282182	14	−18.1	2,328
17		0.003084	0.282203	15	−17.4	2,282
19		0.003414	0.282063	15	−22.3	2,590
20		0.002696	0.282217	14	−16.8	2,249
22		0.002303	0.282229	13	−16.3	2,219
23		0.003220	0.282166	13	−18.7	2,364

$\varepsilon_{Hf}(t)$ values of the Shangshuiquan granite are recalculated at 140 Ma. $\varepsilon_{Hf}(t) = 10{,}000\{[(^{176}Hf/^{177}Hf)_S - (^{176}Lu/^{177}Hf)_S \times (e^{\lambda t} - 1)]/[(^{176}Hf/^{177}Hf)_{CHUR,0} - (^{176}Lu/^{177}Hf)_{CHUR} \times (e^{\lambda t} - 1)] - 1\}$; $T_{DM}^{Hf,\ C} = 1/\lambda \times \ln\{1 + [(^{176}Hf/^{177}Hf)_{S,\ t} - (^{176}Hf/^{177}Hf)_{DM,\ t}]/[(^{176}Lu/^{177}Hf)_C - (^{176}Lu/^{177}Hf)_{DM}]\} + t$

[a] The zircon U–Pb ages of xenolith DMP-06 have been reported in Liu et al. (2004)

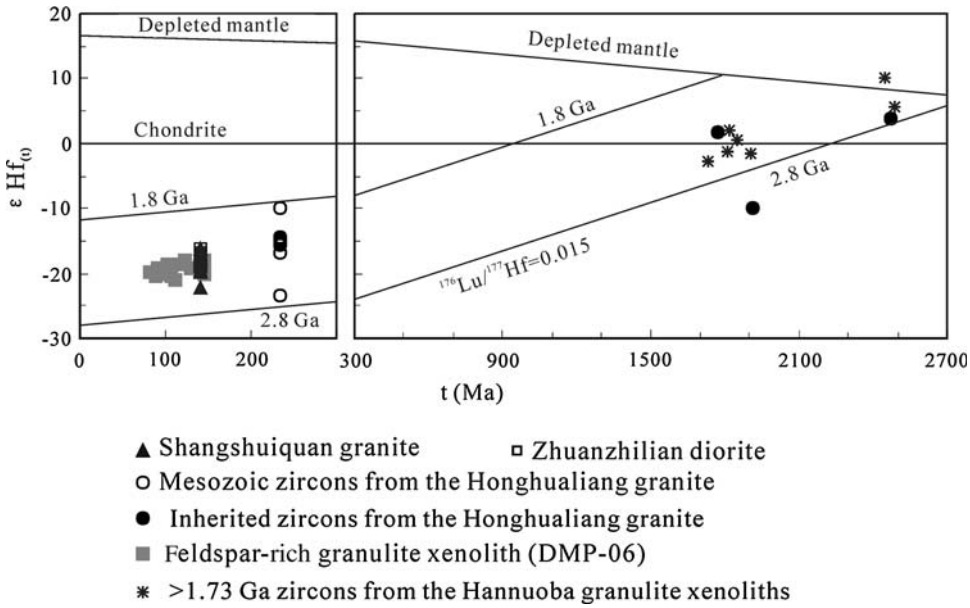

Fig. 8 Age-corrected εHf (*t*) versus ages as *t* (Ma) diagram. Data data of the >1.73 Ga zircons from the Hannuoba mafic granulite xenoliths are from Zheng et al. (2004) and the data of the Zhuanzhilian diorite and the Honghualiang granite are from Jiang et al. (2007)

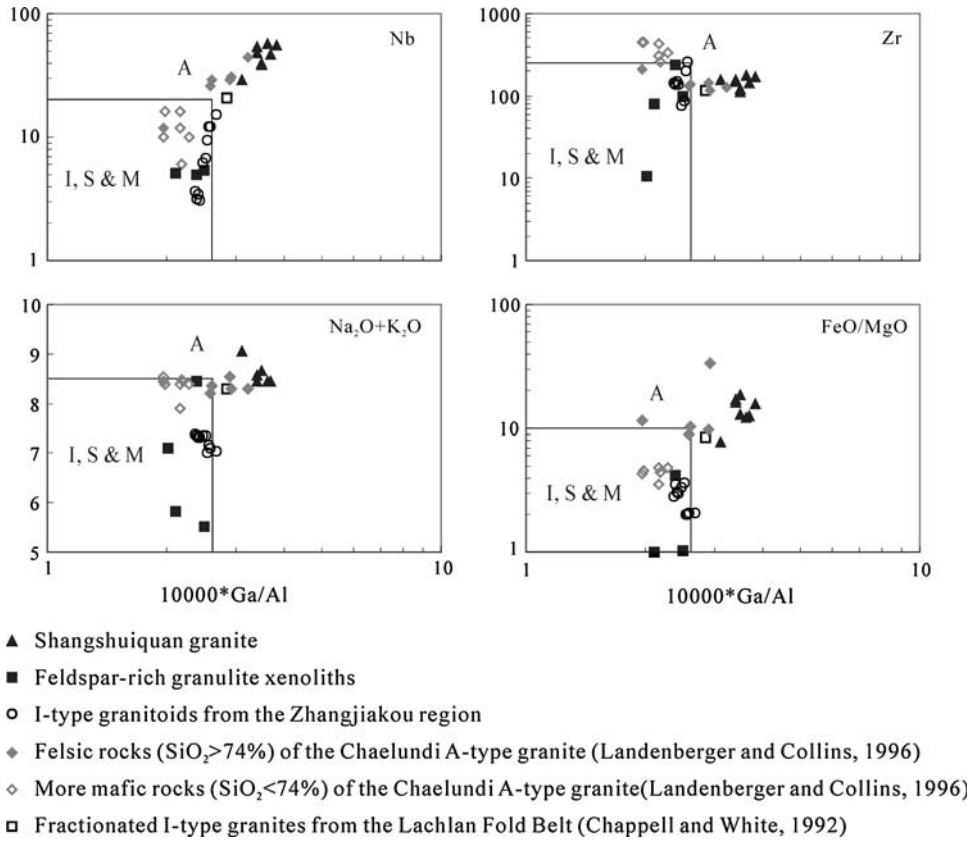

Fig. 9 10,000 Ga/Al versus $(Na_2O + K_2O)/CaO$, FeO_t/MgO, Nb and Zr discrimination diagrams of Whalen et al. (1987). *I, S* and *M* I-, S- and M-type granites, *A* A-type granite

their Cr and Ni concentrations are lower than those of the outcropping amphibolites and granulites which presumably represent the source rocks in the lower crust of most of the granitoids in the region (Jiang et al. 2007), and some of them even lower than those of the Archean basement gneiss sample N48 (Jiang 2005). Therefore, it is unlikely that the feldspar-rich xenoliths are restites left after partial melting of rocks in the lower crust because the restites should be relatively enriched in Cr and Ni. Instead, it would be reasonable to regard them as early cumulates from felsic melts that intrinsically have fairly low concentrations of Cr and Ni. Similarly, a xenolith (85–107) with low Cr and Ni contents from McBride, north Queensland, Austrilia, was interpreted to represent a mafic

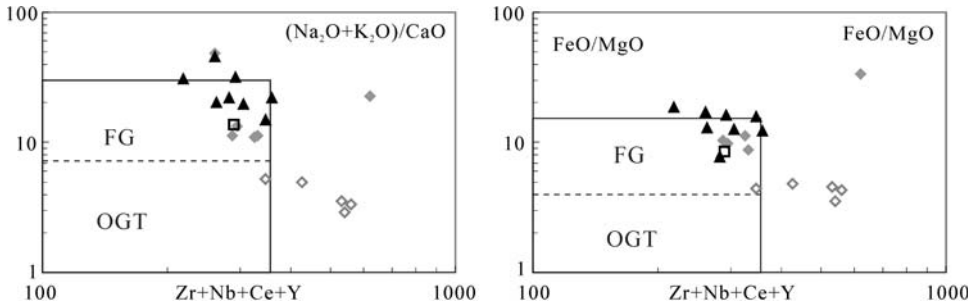

Fig. 10 (Zr + Nb + Ce + Y) versus ($Na_2O + K_2O$)/CaO and FeO/MgO discrimination diagrams of Whalen et al. (1987). *FG* fractionated felsic granites, *OGT* unfractionated I-, S- and M-type granites

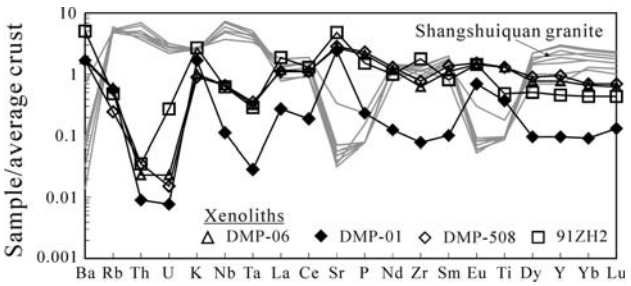

Fig. 11 Multi-element diagram normalized to the bulk crust. Normalizing values from Rudnick and Gao (2003). Source of data is the same as in Fig. 4

cumulate from a granitic magma (Rudnick and Taylor 1987).

When normalized to the average value of bulk crust (Rudnick and Gao 2003), for most elements, the feldspar-rich xenoliths yield sympathetic variations to the granite samples, strongly supporting that the xenoliths are early cumulates (Fig. 11). The strongly negative anomalies of Ba, Sr, P, Eu and Ti in the Shangshuiquan granite require early fractionation of feldspars, apatite and Fe–Ti oxides. These minerals are indeed observed modally in the feldspar-rich xenoliths. In contrast to the highly negative Eu anomaly for the Shangshuiquan granite, the feldspar-rich xenoliths typically have positive Eu anomaly (Eu/Eu* = 6.2 for xenolith DMP-01). Therefore, the large negative Eu anomaly of the Shangshuiquan granite could be caused by fractionation to form the feldspar-rich xenoliths. Again, the high content of Ba precludes that the xenoliths are restites of partial melting because Ba is highly compatible during partial melting.

Sr–Nd isotopes also support a cumulate origin for the feldspar-rich granulite xenoliths. On one hand, the feldspar-rich xenoliths have lower $^{147}Sm/^{144}Nd$ ratios (typically <0.12) than those of the pyroxene-rich xenoliths (typically >0.14) and the exposed granulites and amphibolites (typically >0.12). This is inconsistent with a restite origin for the xenoliths since higher Sm/Nd ratios would be expected in the restites due to enrichment of incompatible elements in the partial melts (hence lower Sm/Nd ratios). On the other hand, the high $^{147}Sm/^{144}Nd$ ratios (up to 0.166) in the Shangshuiquan granite are unusual since the partial melts should have low Sm/Nd ratios, as seen in the Mesozoic I-type granitoids from the region (Jiang et al. 2007). It implies that the high $^{147}Sm/^{144}Nd$ ratios in the Shangshuiquan granite cannot be taken as a primary feature. Instead, it could result from crystal–liquid fractionation. Indeed, early fractionation of LREE (e.g., preferential partitioning of Nd relative to Sm) can account for the low $^{147}Sm/^{144}Nd$ ratios observed in the feldspar-rich xenoliths and the high $^{147}Sm/^{144}Nd$ ratios in the Shangshuiquan granite. The high $^{147}Sm/^{144}Nd$ ratios of the Shangshuiquan granite lead to unrealistically older T_{DM}^{Nd} model ages (Table 3), whereas the low $^{147}Sm/^{144}Nd$ ratios of the feldspar-rich xenoliths result in younger T_{DM}^{Nd} model ages than those of the pyroxene-rich xenoliths and the exposed granulites and amphibolites (2.6–2.8 Ga, Jiang et al. 2007). Despite of contrasting $^{147}Sm/^{144}Nd$ ratios, the Shangshuiquan granite and the feldspar-rich xenoliths have similar $\varepsilon_{Nd}(t)$ values (Fig. 6), strongly supporting derivation from the same partial melts. Therefore, the feldspar-rich xenoliths are best explained as early cumulates rather than residua. Furthermore, the Shangshuiquan granite and the feldspar-rich xenoliths have similar initial $(^{87}Sr/^{86}Sr)_t$ ratios but different Rb/Sr ratios, also consistent with our suggestion (Fig. 6). Higher Rb/Sr ratios in the Shangshuiquan granite could also be attributed to preferential fractionation of Sr (relative to Rb) into the xenoliths.

Zircon U–Pb ages provide additional evidence for our proposal. A number of zircon grains from feldspar-rich xenolith DMP-06 have U–Pb ages between 143 and 146 Ma (Table 4). Similar ages are also found in xenolith DMP-508 (Liu et al. 2004). Besides these ages, most zircons from the two xenoliths have ages between 90 and 140 Ma. The older zircon ages were considered to reflect original igneous crystallization while the younger ones represent subsequent metamorphism (Liu et al. 2004). However, there are no differences between zircons of various ages in morphology, internal structure and Th/U ratios. A large span in U–Pb ages from 340 to 240 Ma was also observed for the mafic xenolith 85–107 from McBride, Northern Queensland, Australia, which was interpreted as cumulate from a granitic magma and the range of U–Pb ages have been attributed to Pb loss (Rudnick and Taylor

1987). Whether the large span of zircon U–Pb ages for the feldspar-rich xenoliths reflects igneous crystallization and sequent metamorphism or Pb loss is beyond the scope of the work. If the 143–146 Ma zircon ages could represent the initial crystallization age for the xenoliths, they are slightly older than the age of the Shangshuiquan granite. This is consistent with earlier crystallization of the xenoliths. From this aspect, the feldspar-rich xenoliths are most likely early cumulates of the Shangshuiquan granite.

Finally, in situ Hf isotope data for zircons provide strong evidence for the linkage between the Shangshuiquan granite and the feldspar-rich xenoliths. The initial Hf isotope values of the zircons from the Shangshuiquan granite and the feldspar-rich xenolith are essentially identical and they are similar to those of the Mesozoic zircons from the I-type granitoids. In fact, they all fall in the field defined by the 1.8 and 2.8 Ga evolution trend of the ancient lower crust (Fig. 8), indicating that all the Mesozoic zircons may have crystallized from magmas derived from the ancient lower crust.

In summary, the feldspar-rich granulite xenoliths can be regarded as the early cumulates of the Shangshuiquan granite in terms of their mineralogy, chemistry, Sr–Nd isotopes and zircon U–Pb ages and Hf isotopes.

Because the Zhuanzhilian diorite is essentially coeval with the Shangshuiquan granite, it is important to determine whether the diorite represents early fractionated rocks of the granite. No positive Eu anomalies are observed in the diorite (Jiang et al. 2007), arguing against the diorite as early fractionated rocks of the granite. One may also argue that the feldspar-rich xenoliths represent early fractionated rocks of the diorite. There are several lines of evidence arguing against this possibility. First, some of the feldspar-rich xenoliths (e.g. 91ZH2 and DMP-01) have higher SiO_2 than the diorite, precluding the xenoliths as early fractionated rocks of the diorite. Second, although the feldspar-rich xenoliths have much higher MgO and Mg# than the diorite, their Cr and Ni concentrations are lower than those of the diorite. Third, clinopyroxene in the xenoliths has lower MgO and Mg# than that in the Zhuanzhilian diorite (Jiang et al. 2007). Finally, there are no Sr, P, Ti and Eu anomalies observed in the diorite (Jiang et al. 2007), arguing against that the diorite has undergone significant fractionation. Therefore, it is precluded that the feldspar-rich xenoliths represent early fractionated rocks from the diorite.

Comparison with the Chaelundi A-type suite, eastern Australia

Overall, the Shangshuiquan granite is similar to the leucogranites of the Chaelundi A-type suite, eastern Australia (Landenberger and Collins 1996). The leucogranites of the Chaelundi A-type suite have the same mineralogy as the Shangshuiquan granite. Geochemically, they are also remarkably similar (e.g., a large negative Eu anomaly and flat REE pattern). The Chaelundi leucogranites have been demonstrated to be highly fractionated from the more mafic member of the A-type suite (Landenberger and Collins 1996). In addition, augite, hypersthene and calcic plagioclase occur as small mafic 'clots' or single crystals in the more mafic member of the Chaelundi A-type suite. Such a mineral assemblage is strikingly similar to that of the Hannuoba feldspar-rich granulite xenoliths. They may represent early cumulus minerals of the Chaelundi A-type suite. For comparison, it is likely that the Shangshuiquan granite is a highly fractionated product and the Hannuoba feldspar-rich granulite xenoliths represent the early cumulates.

Parental magmas

Although it is reasonable to consider that the Hannuoba feldspar-rich granulite xenoliths and the Shangshuiquan granite may respectively represent the cumulates and the residual liquid from fractional crystallization in terms of geochemistry, isotopic composition and ages, it is impossible to determine the compositions of the parental magmas of the Shangshuiquan granite because we are uncertain to what extent the fractionation has taken place. Nevertheless, given the Shangshuiquan granite is mineralogically and geochemically similar to the Chaelundi leucogranites, we can estimate the compositions of the parental magmas by assuming that the degree of fractionation is similar to that of the Chaelundi A-type suite ($\sim$70%, Landenberger and Collins 1996). The calculation assumes that the feldspar-rich xenoliths represent early cumulates and the least evolved sample of the Shangshuiquan granite (JN0749) represents the fractionated end-member. The assumption is substantiated by the similarity between the zircon and apatite saturation temperatures for sample JN0749 and the temperatures based on two-pyroxene geothermometer for the xenoliths (Tables 2, 3).

For major element modeling, mass-balance equation is used:

Parental melts = felsic end-member
+ fractionated cumulates.

By comparison with the Chaelundi A-type suite, the felsic end-member represented by sample JN0749 is assumed to be produced by 65% fractionation of the parent magmas. The fractionated phases include clinopyroxene, orthopyroxene, plagioclase, K-feldspar, quartz, ilmenit and magnetite, all of which are observed in the feldspar-rich xenoliths. The results show that the

Table 5 Major element modeling

	Shangshuiquan granite			Feldspar-rich xenoliths (normalized)		Chaelundi A-type suite		
	Daughter JN0749	Cumulate	Parent	91ZH2[a]	DMP-01[a]	Parent CC131	Cumulate	Daughter CC57
Major element (%)								
SiO_2	74.68	62.35	66.94	62.42	62.13	66.75	62.39	75.69
TiO_2	0.13	0.43	0.33	0.35	0.28	0.62	1.0	0.10
Al_2O_3	13.03	17.07	15.71	19.42	17.08	15.63	17.33	13.00
ΣFeO	1.32	3.48	2.72	3.77	3.67	3.67	5.81	1.06
MnO	0.03	0.07	0.06	0.06	0.07	0.08	0.12	0.04
MgO	0.17	2.47	1.67	0.89	5.11	1.05	1.83	0.11
CaO	0.41	4.43	3.02	4.40	4.33	2.7	4.18	0.64
Na_2O	4.12	4.49	4.38	3.72	4.13	4.26	4.71	4.10
K_2O	4.92	4.68	4.78	4.97	3.19	3.63	2.63	4.45

The modeling assumes that the felsic end-member as represented by sample JN0749 is produced by 65% fractionation of the parent magmas. The modal mineralogy of the fractionated phases is 0.09Cpx + 0.07Opx + 0.4Pl + 0.38Ksp + 0.05 Qtz + 0.003 Ilm + 0.007Mt. The mineral chemistry of xenolith DMP-01 is used (Table 2)

[a] Data of the feldspar-rich xenoliths are from Zhang (1997) and Liu et al. (2001). Data of the Chaelundi A-type suite are from Landenberger and Collins (1996)

calculated cumulate is chemically similar to xenoliths DMP-01 and 91ZH2 and both the calculated cumulate and parental magmas are similar to those of the Chaelundi A-type suite (Table 5).

The calculated parental magma is enriched in Al_2O_3, Na_2O and K_2O (Table 5; Fig. 12), characteristics of the three nearby Mesozoic I-type granitoids (Jiang et al. 2007). On major element Harker diagrams, except for K_2O and TiO_2, the major elements for the parent magma broadly plot along the trend defined by the three Mesozoic graniotoids (Fig. 12).

For trace element and rare earth element modeling, the equation for Rayleigh fractional crystallization is used:

$$C_1^i = C_0^i f^{(Di-1)}$$

where C_0^i is the concentration of element i in the original melt (parental magma), C_1^i is the concentration of element i in the remaining magma (daughter), f is the fraction of remaining melt and Di is the bulk distribution coefficient for element i.

Trace element and rare earth element concentrations were calculated for the parental magma using the concentration in the felsic end-member (JN0749) together with the fraction of the felsic end-member and mineral proportions in the fractionated xenoliths (Table 5). The mineral proportions used in these calculations are as fractions of the total removed mineralogy.

During the REE modeling, we assume that allanite is involved during the fractionation because xenoliths DMP-01 and 91ZH2 shows higher La_N/Yb_N ratios than rocks of the Shangshuiquan granite. In particular, xenolith 91ZH2 has a very high La_N/Yb_N ratio of 33.7, indicating that LREE-rich mineral (e.g., allanite) may involve during the fractionation. Also, removal of allanite was considered to be responsible for the fall in LREE in the Chaelundi leucogranite and, indeed, allanite is observed in the less fractionated rocks of the Chaelundi A-type suite (Landenberger and Collins 1996). In the REE modeling, we use an arbitrary amount (0.05%) of allanite removed during the fractionation.

The results of trace element modeling show that the parental magma is enriched in Sr and Ba and depleted in Yb and Y and there is a small negative Eu anomaly on chondrite-normalized REE pattern (Table 6; Fig. 13). Again, these features are characteristic of the nearby Mesozoic I-type granitoids (Jiang et al. 2007).

With 65% fractionation, our calculated parental magmas show an overall similarity in major and trace element concentrations as well as Eu anomaly to the presumed parental magma of the Chaelundi A-type suite (Tables 5, 6). However, our parental magmas have significantly higher Sr but lower TiO_2. If minor fractionation of xenoliths DMP-06 and DMP-508 involved, the calculated parental magmas would contain higher TiO_2. Our calculated parental magma has Sr concentration comparable to the nearby I-type granitoids. Similarly, the parental magma of the Chaelundi A-type suite is similar to that of the I-type suite in Sr concentrations. Therefore, we contend that the Sr difference between the parental magma of the Shangshuiquan granite and that of the Chaelundi leucogranites could be attributed to difference in the sources. Moreover, our calculated parental magma is similar to the nearby Mesozoic I-type

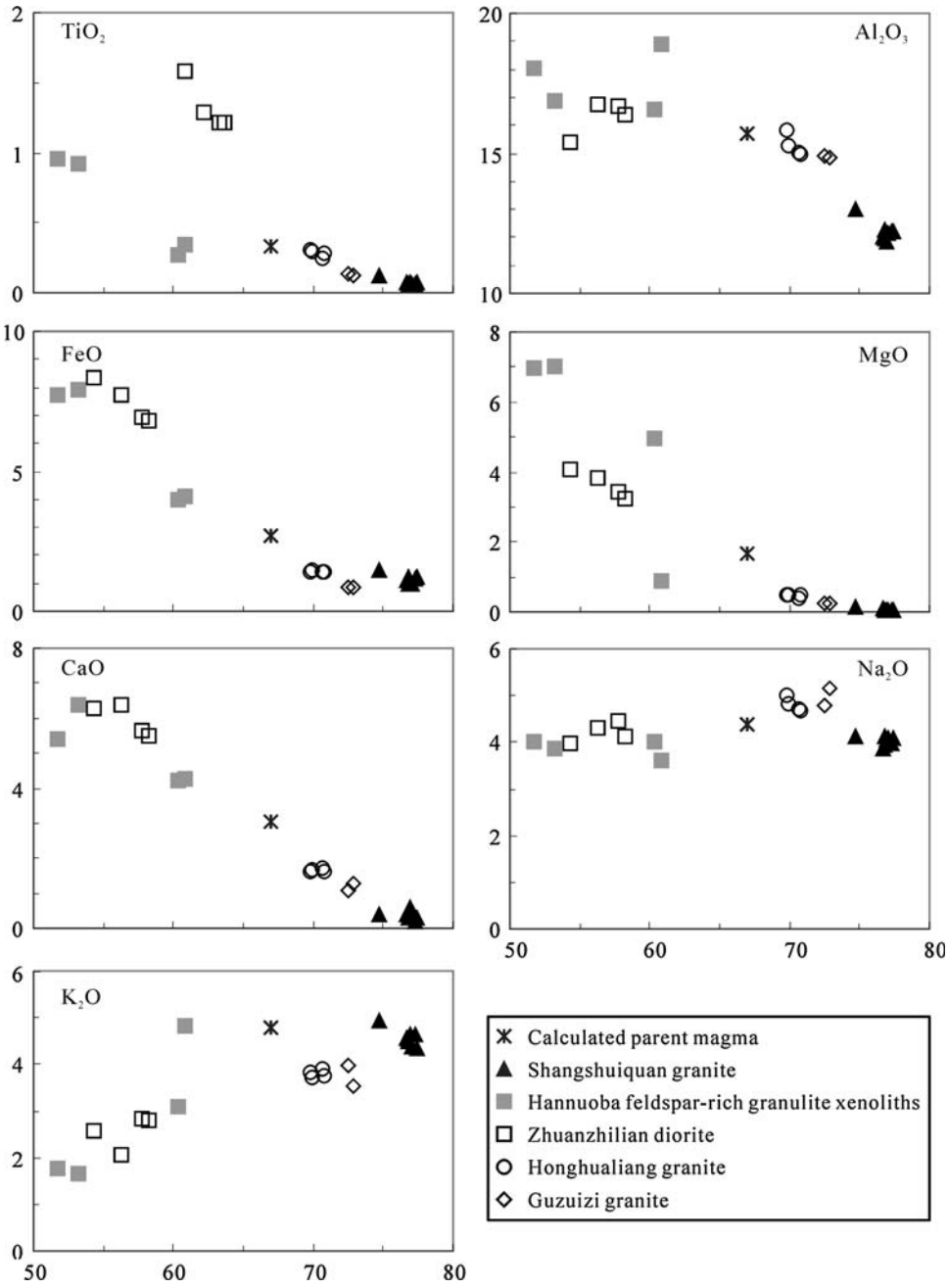

Fig. 12 Harker plots showing the variation of major elements (wt%) for the Shangshuiquan granite, the feldspar-rich xenoliths and the calculated parent magma in comparison with the Mesozoic granitoids from the Zhangjiakou region. Source of data are the same as in Fig. 5

magmas. This is also true for the Chaelundi A- and I-type suites (Landenberger and Collins 1996).

Taken together, the modeling shows that the parent magma of the Shangshuiquan granite is indistinguishable from those of the nearby Mesozoic I-type granitoids in both major and trace element concentrations. Therefore, we consider that the parental magmas for the Shangshuiquan granite are I-type. This is different from Landenberger and Collins (1996) who classify the parental magmas of the Chaelundi leucogranites as A-type. In fact, the more mafic rocks that are assumed to represent the parental magmas of the Chaelundi A-type suite has 10,000 Ga/Al ratio ≤ 2.3 (Fig. 9), significantly lower than the value (>2.6) suggested for A-type granites (Whalen et al. 1987). In this regard, we consider that the parental magmas for the Chaelundi A-type suite may actually be I-type. This may explain why the A-type suite is temporally and spatially associated with the I-type suite and both types of granites have similar geochemical characteristics and identical Sr isotopic compositions (Landenberger and Collins 1996). If this is case, the differences between the two suites could be attributed to differences in source rocks and/or partial

Table 6 Trace element and rare earth element modeling

	Cpx	Opx	Pl	K-spar	Ilm	Mt	Qtz	Aln	Bulk *D*
Partition coefficients used									
Rb	0.032	0.003	0.041	0.34					0.149
Sr	0.516	0.009	4.4	3.87					3.278
Y	4	1	0.1	0.006	2.09				0.479
Nb	0.8	0.8				2.5			0.146
Ba	0.131	0.003	0.308	6.12					2.461
La	0.16	0.11	0.38	0.072	3.6	0.01		820	0.622
Ce	0.21	0.15	0.27	0.044	3.46	0.01		635	0.482
Nd	0.45	0.22	0.21	0.025	3.22	0.01		463	0.391
Sm	0.8	0.27	0.013	0.018	2.83	0.01		2.5	0.113
Eu	0.85	0.17	2.15	1.13	0.55	0.01		81	1.420
Gd	1.1	0.34	0.097	0.011		0.01		130	0.231
Dy	1.45	0.46	0.064	0.006	2.633	0.01			0.199
Er	1.8	0.65	0.055	0.006		0.01			0.232
Yb	1.1	0.86	0.049	0.012	1.64	0.01		8.9	0.193
Lu	1	0.9	0.046	0.006	1.14	0.01		7.7	0.181
Weight fraction used									Liquid fraction
	0.090	0.070	0.400	0.380	0.003	0.007	0.050	0.0005	0.35

	Calculated results		Xenoliths		Chaelundi A-type suite	
	Parent	Daughter	DMP-01	91ZH2	Parent	Daughter
Rb	103.4	253	28	23	93	307
Sr	1,193	109	775	1,500	281	46
Y	10.9	18.9	1.84	8.8	33	80
Nb	11.8	28.9	0.88	5.0	16	29
Ba	1,474	318	774	2,300	908	138
La	24.1	35.8	5.45	38	30	14
Ce	46.9	80.7	8.08	57	62	42
Nd	15.2	28.9	2.44	20	32	25
Sm	2.08	5.27	0.38	3.2	6.33	7.82
Eu	0.52	0.34	0.76	1.6	1.52	0.18
Gd	1.77	3.96	0.37	3.4		
Dy	1.54	3.57	0.34	1.8		
Er	0.90	2.02	0.16	1.0		
Yb	0.96	2.23	0.17	0.81	2.94	8.87
Lu	0.13	0.30	0.04	0.13	0.42	1.4
Eu/Eu*	0.84	0.23	6.20	1.48		
La_N/Yb_N	18.10	11.53	23.0	33.7		

Weight fractions are as fractions of the removed mineralogy. Partition coefficients are from Arth (1976), Brooks et al. (1981), Green and Pearson (1985) and Landenberger and Collins (1996). Data of the Chaelundi A-type suite are from Landenberger and Collins (1996)

melting conditions (e.g., P–T). For example, the considerably higher Zr and other high field strength element (HFSE) in the parental magma of the Chaelundi A-type suite than those of the I-type suite may be caused by higher temperature during partial melting because high field strength element solubility increases with temperature (Watson 1979). Indeed, pyroxenes occur in the A-type suite while they do not occur in the I-type suite, suggesting higher temperature for the former than the later.

Source of the Shangshuiquan granite

The relatively high initial $(^{87}Sr/^{86}Sr)_i$ and low ε_{Nd} (t) values of the Shangshuiquan A-type granite compared with the Hannuoba basalts and peridotite xenoliths clearly exclude mantle as its magma source. Therefore, an origin of highly fractionated products of mantle-derived mafic magmas (Turner et al. 1992; Volkert et al. 2000; Mushkin et al. 2003) is not considered here.

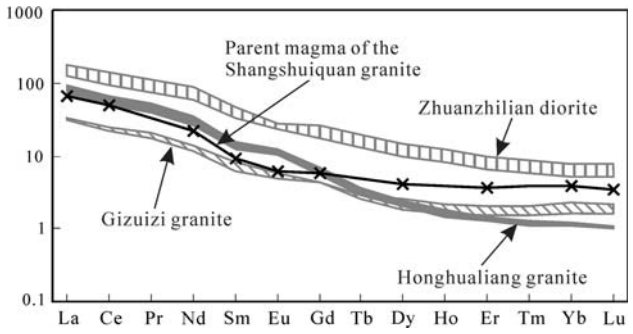

Fig. 13 Chondrite-normalized REE patterns of the calculated parental magma for the Shangshuiquan granite in comparison with the Mesozoic granitoids. Normalizing values from Sun and McDonough (1989)

One may argue that the Shangshuiquan granite formed by interaction between mantle-derived basaltic melts and the lower crust. This suggestion is not favored by comparison with the I-type granitoids. Based on whole rock Sr–Nd isotopic and zircon Hf isotopic compositions, occurrence of inherited zircons as well as lack of coexisting, related basaltic and intermediate rocks, the two Triassic granites have been considered to be derived from the ancient lower crust (Jiang et al. 2007). Since the Shangshuiquan granite is similar to the two Triassic granites in Sr–Nd and zircon Hf isotopic compositions (Figs. 6, 8), we consider a lower crustal magma source is most plausible and a mantle component, if any, is not important. Existence of an ancient lower crust in the studied region has been addressed in detail by Jiang et al. (2007). The Hf isotope values of zircons from the Shangshuiquan granite fall on the evolution trend of those of the inherited zircons from the Honghualiang granite and of the >1.73 Ga zircons from the mafic granulite xenoliths (Zheng et al. 2004) (Fig. 8). Therefore, it is reasonable to deduce that the Shangshuiquan granite is derived from the ancient lower crust. In other words, the Shangshuiquan granite has a common lower crustal source to that of the I-type granitoids.

Although based on Sr–Nd–Hf isotopes we consider that the Shangshuiquan granite has a similar source to the Mesozoic I-type granitoids, it by no means indicates that they all are derived from the same source. In fact, the source rocks for the three I-type granitoids have been considered chemically different (Jiang et al. 2007). All these rocks reflect the heterogeneity of the lower crust.

The felsic granulite xenoliths from Hannuoba and exposed felsic granulites and granulite-facies metasediments typically have $(^{87}Sr/^{86}Sr)_i > 0.72$ and $\varepsilon_{Nd}(t) < -20$ when calculated at 140 Ma (Liu et al. 2004), considerably different from those of the Shangshuiquan granite. Therefore, felsic granulites and granulite-facies metasediments are unlikely the source rocks of the Shangshuiquan granite. In other words, the source rocks are most likely intermediate-mafic, metaigneous rocks.

Implications for the origin of granulite xenoliths

Zircons in lower crustal granulite xenoliths commonly have different age populations (Rudnick and Taylor 1987; Wilde et al. 2003; Huang et al. 2004; Liu et al. 2004). However, interpretation of such age populations in terms of process is not straightforward. For example, zircons in the Hannuoba mafic and intermediate granulite xenoliths are dominated by Mesozoic ages with subordinate Precambrian ages (Wilde et al. 2003; Liu et al. 2004), significantly younger than the Archean age of the granulite terrains in the region. While some have considered these granulite xenoliths to be derived from Mesozoic basaltic underplating (Chen et al. 2001; Zhou et al. 2002; Huang et al. 2004; Liu et al. 2004), some others interpreted them to represent portions of the ancient lower crust (Wilde et al. 2003). Our Hf isotopic compositions of Mesozoic zircons from the feldspar-rich xenoliths unambiguously indicate that these xenoliths may have been derived from the ancient lower crust, rather than from Mesozoic basaltic underplating as suggested previously (Zhou et al. 2002; Huang et al. 2004; Liu et al. 2004). Therefore, zircon crystallization ages alone cannot fully reveal the origin of the xenoliths, unless these are augmented by in situ Lu–Hf isotope systematics. In this regard, the implications of different age populations of granulite xenoliths from many other regions need to be re-evaluated. Whether these zircons of different ages are derived from newly underplated magmas or from the pre-existing crust could be tested by analysis of Hf isotopes in the dated zircons.

Although the feldspar-rich granulite xenoliths and the pyroxene-rich granulite xenoliths at Hannuoba have similar Sr–Nd isotope compositions, they are considered to have different origins. Some of the pyroxene-rich xenoliths have been regarded as restites of the Mesozoic granitoids (Jiang et al. 2007). In this paper, some of the feldspar-rich xenoliths are explained to represent early cumulates of the Shangshuiquan granite. Yet, the Hannuoba granulite xenoliths by no means have only these two origins. Some xenoliths may be portions of the ancient lower crust nearly unaffected by later thermal events. This may be represented by two Hannuoba mafic granulite xenoliths that contain zircons exclusively older than 1.73 Ga (Zheng et al. 2004). Obviously, no a single process is appropriate for the origin of the Hannuoba granulite xenoliths. Our results show that an integrated study of the granulite xenoliths, the granulite terrains and related magmatism can put better constrains on the origin of granulite xenoliths. This approach can be applied to other regions.

Conclusions

The Shangshuiquan granite is derived by partial melting of the ancient lower crust. Its parent magmas are probably I-type and its A-type characteristics are the results of extensive fractionation. Some of the Hannuoba feldspar-rich xenoliths can be regarded as the early cumulates rather than mantle-derived magmas underplated in the Mesozoic as suggested previously (Chen et al. 2001; Zhou et al. 2002; Huang et al. 2004; Liu et al. 2004). It is inferred that many of the granites regarded as 'A-type', especially those lacking close relationship with unfractionated rocks, may be in fact fractionated, felsic I-type granites. This may explain why many I- and A-type granites are temporally and spatially associated and display similar Sr–Nd isotopic compositions in many areas (King et al. 1997; Wu et al. 2002; Zhang et al. 2008).

Acknowledgments Qian Mao and Yuguang Ma are thanked for help in cathodoluminescence imaging and Zhuyin Chu, Chaofeng Li, Haihong, Chen, Zhaochu Hu, Xindi Jin, Liewen Xie and Yueheng Yang are thanked for helps during Sr and Nd isotope, zircon LA-ICP-MS age, ICP-MS, XRF and zircon Hf isotope analyses. This research was supported by the Ministry of Science and Technology, China (grant 2006CB403504) and the National Natural Science Foundation of China (No. 40773024).

References

Arth JG (1976) Behavior of trace elements during magmatic processes—a summary of theoretical models and their applications. J Res US Geol Surv 4:41–47

Barbarin B (1999) A review of the relationships between granitoid types, their origins and their geodynamic environments. Lithos 46:605–626. doi:10.1016/S0024-4937(98)00085-1

Blichert-Toft J, Albarede F (1997) The Lu–Hf isotope geochemistry of chondrites and the evolution of the mantle–crust system. Earth Planet Sci Lett 148:243–258. doi:10.1016/S0012-821X(97)00040-X

Brooks CK, Henderson P, Ronsbo JG (1981) Rare earth element partitioning between allanite and glass in the obsidian of Sandy Bracs, Northern Ireland. Mineral Mag 44:157–160. doi:10.1180/minmag.1981.044.334.07

Chappell BW, White AJR (1974) Two contrasting granite types. Pac Geol 8:173–174

Chappell BW, White AJR (1992) I- and S-type granites in the Lachlan Fold Belt. Trans R Soc Edinb Earth Sci 83:1–26

Chen SH, Zhang GH, Zhou XH, Sun M, Feng JL, Xie MZ (1998) Petrological investigation on the granulite xenoliths from Hannuoba basalts, northern Sino-Korean craton. Acta Petrol Sin 14:366–380 (in Chinese)

Chen SH, O'Reilly SY, Zhou XH, Griffin WL, Zhang GH, Sun M, Feng JL, Zhang M (2001) Thermal and petrological structure of the lithosphere beneath Hannuoba, Sino-Korean craton, China: evidence from xenoliths. Lithos 56:267–301. doi:10.1016/S0024-4937(00)00065-7

Collins WJ, Beams SD, White AJR, Chappell BW (1982) Nature and origin of A-type granites with particular reference to southeastern Australia. Contrib Mineral Petrol 80:189–200. doi:10.1007/BF00374895

Creaser RA, Price RC, Wormald RJ (1991) A-type granites revisited: assessment of a residual-source model. Geology 19:163–166. doi:10.1130/0091-7613(1991)019<0163:ATGRAO>2.3.CO;2

Eby GN (1990) A-type granitoids: a review of their occurrence and chemical characteristics and speculations on their petrogenesis. Lithos 26:115–134. doi:10.1016/0024-4937(90)90043-Z

Frost BR, Barnes CG, Collins WJ, Arculus RJ, Ellis DJ, Frost CD (2001) A geochemical classification for granitic rocks. J Petrol 42:2033–2048. doi:10.1093/petrology/42.11.2033

Goldstein SL, O'Nions RK, Hamilton PJ (1984) A Sm–Nd isotopic study of atmospheric dusts and particulates from major river system. Earth Planet Sci Lett 70:221–236. doi:10.1016/0012-821X(84)90007-4

Green TH, Pearson NJ (1985) Rare earth element partitioning between clinopyroxene and silicate liquid at moderate to high pressure. Contrib Mineral Petrol 91:24–26. doi:10.1007/BF00429424

Griffin WL, Zhang AD, O'Reilly SY, Ryan CG (1998) Phanerozoic evolution of the lithosphere beneath the Sino-Korean craton. In: Flower M, Chung SL, Lo CH, Lee TY (eds) Mantle Dynamics and Plate Interactions in East Asia. American Geophysical Union, Geodynamic Series 27, pp 107–126

Griffin WL, Wang X, Jackson SE, Pearson NJ, O'Reilly SY (2002) Zircon geochemistry and magma mixing, SE China: in situ analysis of Hf isotopes, Tonglu and Pingtan igneous complexes. Lithos 61:237–269. doi:10.1016/S0024-4937(02)00082-8

Harrison TM, Watson EB (1984) The behavior of apatite during crustal anatexis: equilibrium and kinetic considerations. Geochim Cosmochim Acta 48:1467–1477. doi:10.1016/0016-7037(84)90403-4

Huang XL, Xu YG, Liu DY (2004) Geochronology, petrology and geochemistry of the granulite xenoliths from Nushan, east China: Implication for a heterogeneous lower crust beneath the Sino-Korean Craton. Geochim Cosmochim Acta 68:127–149. doi:10.1016/S0016-7037(03)00416-2

Jacobsen SB, Wasserburg GJ (1980) Sm–Nd isotopic evolution of chondrites. Earth Planet Sci Lett 50:139–155. doi:10.1016/0012-821X(80)90125-9

Jiang N (2005) Petrology and geochemistry of the Shuiquangou syenitic complex, northern margin of the North China craton. J Geo Soc Lond 162:203–215. doi:10.1144/0016-764903-144

Jiang N, Liu YS, Zhou WG, Yang JH, Zhang SQ (2007) Derivation of Mesozoic adakitic magmas from ancient lower crust in the North China craton. Geochim Cosmochim Acta 71:2591–2608. doi:10.1016/j.gca.2007.02.018

King PL, White AJR, Chappell BW, Allen CM (1997) Characterization and origin of aluminous A-type granites from the Lachlan Fold Belt, southeastern Australia. J Petrol 38:371–391. doi:10.1093/petrology/38.3.371

Landenberger B, Collins WJ (1996) Derivation of A-type granites from a dehydration charnockitic lower crust: evidence from the Chaelundi complex, eastern Australia. J Petrol 37:145–170. doi:10.1093/petrology/37.1.145

Liu DY, Nutman AP, Compston W, Wu JS, Shen QH (1992) Remnants of ≥3800 Ma crust in the Chinese part of the Sino-Korean craton. Geology 20:339–342. doi:10.1130/0091-7613(1992)020<0339:ROMCIT>2.3.CO;2

Liu YS, Gao S, Jin SY, Hu SY, Sun M, Zhao ZB, Feng JL (2001) Geochemistry of lower crustal xenoliths from Neocene Hannuoba basalt, North China craton: implications for petrogenesis and lower crustal composition. Geochim Cosmochim Acta 65:2589–2604. doi:10.1016/S0016-7037(01)00609-3

Liu YS, Gao S, Yuan HL, Zhou L, Liu XM, Wang XC, Hua ZC, Wang LS (2004) U–Pb zircon ages and Nd, Sr, and Pb isotopes of lower crustal xenoliths from North China Craton: insights on evolution of lower continental crust. Chem Geol 211:87–109. doi:10.1016/j.chemgeo.2004.06.023

Liu YS, Gao S, Lee C-TA, Hu SY, Liu XM, Yuan HL (2005) Melt-peridotite interactions: links between garnet pyroxenite and high-Mg# signature of continental crust. Earth Planet Sci Lett 234:39–57. doi:10.1016/j.epsl.2005.02.034

Loiselle MC, Wones DR (1979) Characterization and origin of anorogenic granites. Geol Soc Am Abstr 11:468

Ludwig KR (2003) User's manual for ISOPLOT 3.00: a geochronological toolkit for Microsoft Excel, Special Publication No. 4. Berkeley Geochronology Center, p 71

Lugmair GW, Marti K (1978) Lunar initial $^{143}Nd/^{144}Nd$: differential evolution of the lunar crust and mantle. Earth Planet Sci Lett 39:349–357. doi:10.1016/0012-821X(78)90021-3

Menzies A, Fan WM, Zhang M (1993) Paleozoic and Cenozoic lithoprobes and the loss of >120 km of Archean lithosphere, Sino-Korean craton, China. In: Prichard HM, Alabaster T, Harris, NBW, Neary CR (eds) Magmatic processes and plate tectonic. Geological Society, London, pp 71–81

Miao LC, Qiu YM, McNaughton NJ, Luo ZK, Groves DI, Zhai YS, Fan WM, Zhai MG, Guan K (2002) SHRIMP U–Pb zircon geochronology of granitoids from Dongping area, Hebei Province, China: constraints on tectonic evolution and geodynamic setting for gold metallogeny. Ore Geol Rev 19:187–204. doi:10.1016/S0169-1368(01)00041-5

Mushkin A, Navon O, Halicz L, Hartmann G, Stein M (2003) The petrogenesis of A-type magmas from the Amram Massif, southern Israel. J Petrol 44:815–832. doi:10.1093/petrology/44.5.815

Rudnick RL, Gao S (2003) Composition of the continental crust. In: Rudnick RL (ed) The crust, treatise in geochemistry, vol 3, pp 1–64

Rudnick RL, Taylor SR (1987) The composition and petrogenesis of the lower crust: a xenolith study. J Geophys Res 92(B13):13981–14005. doi:10.1029/JB092iB13p13981

Rudnick RL, Gao S, Ling WL, Liu YS, McDonough WF (2004) Petrology and geochemistry of spinel peridotite xenoliths from Hannuoba and Qixia, North China craton. Lithos 77:609–637. doi:10.1016/j.lithos.2004.03.033

Soderlund U, Patchett PJ, Vervoort JD, Isachsen CE (2004) The ^{176}Lu decay constant determined by Lu–Hf and U–Pb isotope systematics of Precambrian mafic intrusions. Earth Planet Sci Lett 219:311–324. doi:10.1016/S0012-821X(04)00012-3

Song Y, Frey FA, Zhi XC (1990) Isotopic characteristics of Hannuoba basalts, Eastern China—implications for their petrogenesis and the composition of subcontinental mantle. Chem Geol 88:35–52. doi:10.1016/0009-2541(90)90102-D

Sun SS, McDonough WF (1989) Chemical and isotopic systematics of oceanic basalts: implications for mantle composition and processes. In: Saunders AD, Norry MJ (eds) Magmatism in ocean basins, vol 42. Geological Society of London, Special Publications, pp 313–345

Turner SP, Foden JD, Morrison RS (1992) Derivation of some A-type magmas by fractionation of basaltic magma; an example from the Padthaway Ridge, South Australia. Lithos 28:151–179. doi:10.1016/0024-4937(92)90029-X

Volkert RA, Feigenson MD, Patino LC, Delaney JS, Drake AA Jr (2000) Sr and Nd isotopic compositions, age and petrogenesis of A-type granitoids of the Vernon Supersuite, New Jersey Highlands, USA. Lithos 50:325–347. doi:10.1016/S0024-4937(99)00065-1

Watson EB (1979) Zircon saturation in felsic liquids: experimental data and applications to trace element geochemistry. Contrib Mineral Petrol 70:407–419. doi:10.1007/BF00371047

Watson EB, Harrison TM (1983) Zircon saturation revisited: temperature and composition effects in a variety of crustal magma types. Earth Planet Sci Lett 64:295–304. doi:10.1016/0012-821X(83)90211-X

Whalen JB, Currie KL, Chappell BW (1987) A-type granites: geochemical characteristics, discrimination and petrogenesis. Contrib Mineral Petrol 95:407–419. doi:10.1007/BF00402202

Wilde SA, Zhou XH, Nemchin AA, Sun M (2003) Mesozoic crust-mantle interaction beneath the North China craton: a consequence of the dispersal of Gondwanaland and accretion of Asia. Geology 31:817–820. doi:10.1130/G19489.1

Wood BJ, Banno S (1973) Garnet-orthopyroxene and orthopyroxene–clinopyroxene relationships in simple and complex systems. Contrib Mineral Petrol 42:109–124. doi:10.1007/BF00371501

Woodhead J, Hergt J, Shelley M, Eggins S, Kemp R (2004) Zircon Hf-isotope analysis with an excimer laser, depth profiling, ablation of complex geometries, and concomitant age estimation. Chem Geol 209:121–135. doi:10.1016/j.chemgeo.2004.04.026

Wu FY, Sun DY, Li HM, Jahn BM, Wilde SA (2002) A-type granites in northeastern China: age and geochemical constraints on their petrogenesis. Chem Geol 187:143–173. doi:10.1016/S0009-2541(02)00018-9

Wu FY, Yang YH, Xie LW, Yang JH, Xu P (2006) Hf isotopic compositions of the standard zircons and baddeleyites used in U–Pb geochronology. Chem Geol 234:105–126. doi:10.1016/j.chemgeo.2006.05.003

Yuan HL, Gao S, Liu XM, Li HM, Günther D, Wu FY (2004) Accurate U–Pb age and trace element determinations of zircon by laser ablation-inductively coupled plasma mass spectrometry. Geostand Newsl 28:353–370. doi:10.1111/j.1751-908X.2004.tb00755.x

Zhai MG (1996) Granulites and lower continental crust in North China Archean Craton. Seismological Press, Beijing

Zhang GH (1997) Geochemistry of granulite and pyroxenite xenoliths in Hannuoba basalts, North China, and its implications to crust–mantle interaction. PhD dissertation (Institute of Geology and Geophysics, Chinese Academy of Sciences), p 73 (in Chinese)

Zhang XH, Mao Q, Zhang HF, Wilde SA (2008) A Jurassic peraluminous leucogranite from Yiwulüshan, western Liaoning, North China craton: age, origin and tectonic significance. Geol Mag 145:305–320. doi:10.1017/S0016756807004311

Zhao GC, Wilde SA, Cawood PA, Sun M (2001) Archean blocks and their boundaries in the North China craton: lithological, geochemical, structural and P–T constraints and tectonic evolution. Precambrian Res 107:45–73. doi:10.1016/S0301-9268(00)00154-6

Zheng JP, Lu FX, Yu CM, Tang HY (2004) An in situ zircon Hf isotopic, U–Pb age and trace element study of banded granulite xenolith from Hannuoba basalt: Tracking the early evolution of the lower crust in the North China craton. Chin Sci Bull 49:277–285. doi:10.1360/03wd0385

Zhou XH, Sun M, Zhang GH, Chen SH (2002) Comtinental crust and lithospheric mantle interaction beneath North China: isotopic evidence from granulite xenoliths in Hannuoba, Sino-Korean craton. Lithos 62:111–124. doi:10.1016/S0024-4937(02)00110-X